Resonant Auger decay induced by the symmetry-forbidden 1a1g → 6a1g transition of the SF6 molecule

Antonio Santos, Oksana Travnikova, Nacer Boudjemia, Tatiana Marchenko, Renaud Guillemin, Iyas Ismail, Dimitris Koulentianos, Denis Céolin, Faris Gel'Mukhanov, Marc Simon, et al.

▶ **To cite this version:**

Antonio Santos, Oksana Travnikova, Nacer Boudjemia, Tatiana Marchenko, Renaud Guillemin, et al.. Resonant Auger decay induced by the symmetry-forbidden 1a1g → 6a1g transition of the SF6 molecule. Journal of Vacuum Science & Technology A, 2022, Special Collection: Commemorating the Career of David Arthur Shirley, 40 (4), pp.042801. 10.1116/6.0001890 . hal-03797323

HAL Id: hal-03797323
https://hal.science/hal-03797323

Submitted on 5 Oct 2022

HAL is a multi-disciplinary open access archive for the deposit and dissemination of scientific research documents, whether they are published or not. The documents may come from teaching and research institutions in France or abroad, or from public or private research centers.

L'archive ouverte pluridisciplinaire **HAL**, est destinée au dépôt et à la diffusion de documents scientifiques de niveau recherche, publiés ou non, émanant des établissements d'enseignement et de recherche français ou étrangers, des laboratoires publics ou privés.

JVST A
Journal of Vacuum Science & Technology A

Resonant Auger decay induced by the symmetry-forbidden $1a_{1g} \rightarrow 6a_{1g}$ transition of the SF_6 molecule

Cite as: J. Vac. Sci. Technol. A **40**, 042801 (2022); https://doi.org/10.1116/6.0001890
Submitted: 29 March 2022 • Accepted: 02 May 2022 • Published Online: 25 May 2022

A. C. F. Santos, O. Travnikova, N. Boudjemia, et al.

COLLECTIONS

Paper published as part of the special topic on Commemorating the Career of David Arthur Shirley

View Online Export Citation CrossMark

ARTICLES YOU MAY BE INTERESTED IN

Perspectives on UV and x-ray photoelectron spectroscopy
Journal of Vacuum Science & Technology A **40**, 043002 (2022); https://doi.org/10.1116/6.0001856

Who were the founders of synchrotron radiation? Historical facts and misconceptions
Journal of Vacuum Science & Technology A **40**, 033204 (2022); https://doi.org/10.1116/6.0001686

High synergy atomic layer etching of AlGaN/GaN with HBr and Ar
Journal of Vacuum Science & Technology A **40**, 042601 (2022); https://doi.org/10.1116/6.0001862

© 2022 Author(s).

JVST A
Journal of Vacuum Science & Technology A

ARTICLE

avs.scitation.org/journal/jva

Resonant Auger decay induced by the symmetry-forbidden $1a_{1g} \rightarrow 6a_{1g}$ transition of the SF_6 molecule

Cite as: J. Vac. Sci. Technol. A 40, 042801 (2022); doi: 10.1116/6.0001890
Submitted: 29 March 2022 · Accepted: 2 May 2022 ·
Published Online: 25 May 2022

View Online Export Citation CrossMark

A. C. F. Santos,[1] O. Travnikova,[2,3] N. Boudjemia,[2,a)] T. Marchenko,[2,3] R. Guillemin,[2,3] I. Ismail,[2,3] D. Koulentianos,[2,4,b)] D. Céolin,[3] F. Gel'mukhanov,[5] M. Simon,[2,3] M. N. Piancastelli,[2,6,c)] and R. Püttner[7]

AFFILIATIONS

[1]Instituto de Física, Universidade Federal do Rio de Janeiro, 21941-972 Rio de Janeiro, RJ, Brazil
[2]Sorbonne Université, CNRS, UMR 7614, Laboratoire de Chimie Physique-Matière et Rayonnement, F-75005 Paris, France
[3]Synchrotron SOLEIL, l'Orme des Merisiers, Saint-Aubin, BP 48, F-91192 Gif-sur-Yvette Cedex, France
[4]Department of Physics, University of Gothenburg, Origovägen 6B, SE-412 96 Gothenburg, Sweden
[5]Theoretical Chemistry and Biology, Royal Institute of Technology, SE-10691 Stockholm, Sweden
[6]Department of Physics and Astronomy, Uppsala University, Box 516 SE-75120 Uppsala, Sweden
[7]Fachbereich Physik, Freie Universität Berlin, Arnimallee 14 D-14195 Berlin, Germany

Note: This manuscript is a part of the Special Topic Collection Commemorating the Career of David Arthur Shirley.
[a)]**Present address:** Nano and Molecular Systems Research Unit, University of Oulu, P.O. Box 3000, FI-90014 Oulu, Finland.
[b)]**Present address:** Center for Free-Electron Laser Science, Deutsches Elektronen-Synchrotron DESY, Notkestraße 85, D-22607 Hamburg, Germany and Department of Physics, Universität Hamburg, Luruper Chaussee 149, D-22761 Hamburg, Germany.
[c)]**Electronic mail:** maria-novella.piancastelli@physics.uu.se

ABSTRACT

Resonant Auger electron spectroscopic study at the symmetry-forbidden $1a_{1g} \rightarrow 6a_{1g}$ excitation below the S K-shell threshold of SF_6 is reported. Partial electron yield and resonant KLL Auger spectra have been measured by using monochromatized undulator synchrotron radiation. By changing the photon energy in small steps, a so-called 2D map is produced. In this map, the dipole-forbidden transition exhibits spectral features (e.g., an S-shaped dispersion relation), which are well known and understood for dipole-allowed transitions. We validate by a theory that for the case of dipole-forbidden transitions, these spectral features can be analyzed in the same way as previously established for the dipole-allowed ones. This approach grants information on the nuclear dynamics in the K-shell core-excited states of SF_6 on the femtosecond (fs) timescale. In particular, for the potential-energy curves of the states S $1s^{-1}6a_{1g}$ and S $2p^{-2}6a_{1g}$, the slopes at the equilibrium distance of the ground state are derived. Symmetry breaking as a result of ultrafast vibronic coupling is revealed by the population of the electronically forbidden excited state.

Published under an exclusive license by the AVS. https://doi.org/10.1116/6.0001890

I. INTRODUCTION

For molecules in the gas phase with strongly dissociative potential energy curves, the promotion of an electron from an inner shell to an empty molecular orbital is able to induce fast nuclear dynamics[1–6] with time scales of the order of a few femtoseconds (fs). In addition, inner-shell excited states are remarkably unstable, which is portrayed by overly short lifetimes, with the range of 10^{-16}–10^{-14} s, while molecular vibrations and rotations usually take place on time scales of the order of 10^{-14}–10^{-12} s. Hence, a competition is expected to be observed between relaxation of the inner-shell core-hole state and nuclear dynamics since the electronic lifetime of an inner-shell hole can be of the same order of magnitude as molecular dissociation times. Core-hole-clock spectroscopies (CHCS) are powerful tools to probe ultrafast nuclear

Published under an exclusive license by the AVS

dynamics through the exploration of both processes through their dependence on the incident photon energy.[2] Examples of CHCS are resonant inelastic x-ray scattering (RIXS) and resonant Auger spectroscopy (RAS). In this work, we focus on RAS around the S K-edge (2480–2490 eV) of the SF_6 molecule and, more specifically, on the dipole-forbidden $1a_{1g} \rightarrow 6a_{1g}$ transition; the $1a_{1g}$ orbital is identical to the S 1s core orbital. Note that the lifetime of deep $1s^{-1}$ core holes like S $1s^{-1}$ and Cl $1s^{-1}$ is of the order of 1 fs.[7] On this timescale, a possible bond elongation is of the order of some 10 mÅ at maximum (see Ref. 8 and results presented below), i.e., no bond breaking occurs during the $1s^{-1}$ core-hole lifetime. Instead, in the case of a dissociative state, the molecular fragments get a first kick that contributes in the subsequent steps of the decay on a timescale of a few fs to a significant bond elongation and finally to dissociation. In more detail, the RAS spectra allow deriving the slopes of the potential-energy curves of the core-hole intermediate and double-core-hole final state, which is an important parameter for wave-packet dynamics calculations along the potential-energy curves.

In molecules, the commonly named "vibronic coupling," i.e., the effective interaction between the electronic and nuclear degrees of freedom, becomes observable when symmetry-forbidden electronic transitions are induced because of the coordinate excitation of asymmetric vibrations.[9] In terms of group theory, the direct product of the symmetries of the excited-state orbital and the excited vibrational quantum has to have a dipole-allowed symmetry. In that case, the intensities can be "allotted" from symmetry-allowed transitions through peculiar normal modes of a specific symmetry, commonly named as "promoting mode"; this process is also known as "intensity borrowing." In the case of SF_6, the dipole-forbidden $1a_{1g} \rightarrow 6a_{1g}$ transition is supported by normal vibrational modes from the t_{1u} and, to a much smaller extent, the t_{2u} irreducible representations of the O_h group.[10]

Resonant excitations below the L-edge and the inner-valence region of SF_6 were studied, in particular, by Shirley's group.[11–13] Electronic transitions related to the S K-edge excitation on the SF_6 molecule have been the subject of investigations in the past. Reynaud *et al.*[14] performed photoabsorption measurements of KL-edge double-core-hole states and Feifel *et al.*[15] $K^{-2}V$ double-core-hole states of SF_6. Nakamatsu and Mukoyama[16] carried out molecular orbital calculations for SF_6 by adopting the discrete variational Xα method. Gomes *et al.*[10] performed PEPICO and PE2PICO studies of SF_6 around the S 1s edge. In the latter work, the authors observed strong fragmentation selectivity in symmetry-forbidden vibronic transitions. The decay properties of resonances around the S K-edge were also reported by Shirley's group.[17]

In this paper, we use resonant Auger spectroscopy, and, more specifically, we study the pseudo-photoabsoption spectrum measured in partial electron yield (PEY) mode as a function of the incident photon energy at the $1a_{1g} \rightarrow 6a_{1g}$ dipole-forbidden resonance of the SF_6 molecule. The RAS provides important information on the molecular dynamics subsequent to $1s^{-1}$ excitation in SF_6. The present data show both line narrowing and anomalous dispersion of the spectral lines, which, in fact, exhibit an S-like dispersion. Up to now, such features were observed and explained only for dipole-allowed transitions. Based on the theoretical description of the processes involved, we show that this approach to obtaining information about molecular dynamics can be extended to dipole-forbidden transitions. This allows us to derive from the experimental spectra the potential-energy slopes of the S $1s^{-1}6a_{1g}$ and $2p^{-2}6a_{1g}$ core-hole states at the equilibrium distance of the ground state.

II. EXPERIMENT

The results were obtained at the French synchrotron radiation facility SOLEIL, at the GALAXIES beamline, with the gas-phase end station dedicated to hard-x-ray photoelectron spectroscopy (HAXPES).[18] A linearly polarized photon beam with energies from 2480 to 2490 eV was produced by a U20 undulator. The beam energy was selected and monochromatized using a Si(111) double-crystal monochromator. The Auger spectra were acquired using a SCIENTA EW4000 analyzer, which collected the electrons along the axis parallel to the beam polarization vector. As discussed in the following, we do not expect that the detection direction has in the present case of SF_6 a significant influence on the Auger spectra; this holds at least for the strong and dipole-allowed transitions, which strongly dominate the spectra. It is well known that atomic Auger spectra of core holes with total angular momentum $j = \frac{1}{2}$ show an isotropic angular dependence.[19] This does not hold for molecules in general. However, molecular sulfur KLL Auger spectra with the L-shell bearing a core hole show a strong atomic character so that for the emitted Auger electron, no significant deviation from an isotropic angular distribution is expected. Certainly, the Auger electron can scatter in a second step at the ligand atoms, which can lead for an oriented molecule to an anisotropic angular dependence. However, due to the high symmetry of the molecule, all components of the dipole operator have the same symmetry (t_{1u}) so that the SF_6 molecule does not have to be oriented for both resonant excitations and ionization. Consequently, possible scattering effects of the Auger electron at the ligands should also be isotropic after averaging over the molecular ensemble. For the dipole-forbidden transition S $1s^{-1} \rightarrow 6a_{1g}$, the situation is less clear since Knie *et al.*[20] showed for the case of participator Auger decay that vibronic coupling has a strong influence on the angular distribution. We cannot rule out such an effect for the present case of spectator Auger decay, but we want to point out that this would influence in the present case only the observed Auger intensities and, therefore, not the present results.

The pass energy of the SCIENTA analyzer was set to 500 eV and a curved slit with a width of 300 μm was adopted, leading to an analyzer resolution of ≅375 meV. Moreover, for the resonant Auger spectra, one has to take into account the photon bandwidth of about 300 meV. In this way, the total spectral resolution for resonant photoelectron lines was about 470 meV, which is narrower than the theoretical S $1s^{-1}$ core-hole lifetime broadening ($2\Gamma_{theo} = 0.59$ eV,[7] $2\Gamma_{exp} = 0.55$ eV;[21] note that throughout this publication Γ describes the half width at half maximum (HWHM) of the Lorentzian broadening due to the lifetime). One should mention that the lifetime broadening of the KLL Auger lines is larger than Γ for the $1s^{-1}$ core hole due to the finite broadening of the S 2p level ($2\Gamma_{theo} = 0.054$ eV).[7] The calibration procedure of the photon energy and the kinetic energy of the electrons was performed in a two-step procedure. In the first step, the photon energy

Published under an exclusive license by the AVS

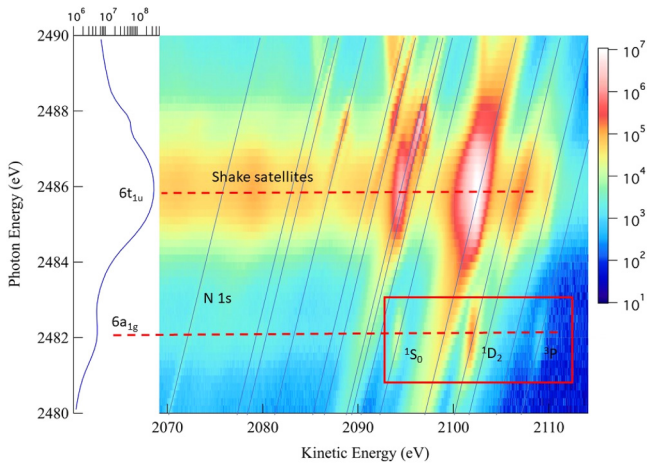

FIG. 1. 2D-map of Auger decay in SF_6 after resonant excitation of the $1a_{1g}$ orbital. The kinetic energy of resonant Auger electrons is shown as a function of the photon energy and the intensity is represented by a logarithmic color scale as shown in the legend on the right side. The diagonal blue lines indicate a linear dispersion for the $2p^{-2}V$ final states. The red box identifies the resonant Auger transitions of interest. The diagonal line marked with N 1s labels the corresponding photoelectron line caused by N_2 impurities in the gas; it was used to calibrate the kinetic energy axis (see text). The PEY spectrum given on a logarithmic scale is plotted on the left side of the 2D-map.

axis of the results shown in Fig. 1 was calibrated by shifting the resonance energy of the $1s^{-1}6t_{1g}$ resonance to the literature value of 2486 eV.[22] In the second step, the N $1s^{-1}$ photoelectron line with a binding energy of ≅409.87 eV[23] (averaged value of the two unresolved components N $1s_g^{-1}$ and N $1s_u^{-1}$) was used to calibrate the kinetic energy axis.

III. EXPERIMENTAL RESULTS

The $1a_{1g}$ molecular orbital is identical to the S 1*s* core orbital of SF_6. The vacant $6a_{1g}$ (LUMO) and $6t_{1u}$ (LUMO+1) orbitals are both antibonding (σ^* type). The two lowest transitions below the S *K*-edge are $1a_{1g} \rightarrow 6a_{1g}$ and $1a_{1g} \rightarrow 6t_{1u}$. For the latter one, the transition is granted by dipole selection rules. On the other hand, in the $1a_{1g} \rightarrow 6a_{1g}$ case, the transition is not dipole-allowed in the O_h symmetry, which does not imply that the magnitude of this transition is rigorously zero, as it can take place through the commonly named "intensity-borrowing mechanism," as discussed in the Introduction.

The physical process we are interested in here consists of the resonant excitation $1a_{1g} \rightarrow 6a_{1g}$ in which a S 1*s* ($1a_{1g}$) electron is promoted to the unoccupied antibonding $6a_{1g}$ orbital, followed by relaxation of the core hole via the resonant *KLL* Auger emission. Information about the interaction of the SF_6 molecule with an x-ray photon can be accessed by exploring the dynamical characteristics of the Auger decay. The specific parameters one can use are the linewidths, energy dispersions, and PEY intensities of the spectral profiles associated with the Auger transitions.

For a general analysis of the present results, it is suitable to show the measured Auger intensities in a 2D-map as a function of the impinging photon energy and the energy of the emitted Auger electron as shown in Fig. 1, in which intensity is described by a color log scale. The PEY spectrum is plotted on the left side of the 2D-map, using also a logarithmic scale to clearly show the positions of the intermediate-state resonances. The measurements were performed in the kinetic energy range of 2070–2115 eV, with 0.05 eV steps. The impinging photon energy was swept from 2480 to 2490 eV using steps of 0.1 eV. The blue lines indicate a linear dispersion with photon energy, which is valid for all $2p^{-2}V$ final states besides the dissociative ones close to the peak maximum. The process of *KLL* Auger decay after resonant S 1*s* excitation can be written as

$$h\nu + SF_6 \rightarrow SF_6^*(1s^{-1}V') \rightarrow SF_6^+(2p^{-2}V) + e_{KLL}^-,$$

where *V* can either mean the LUMO and LUMO+1, which are the $6a_{1g}$ and $6t_{1u}$ orbitals for SF_6, respectively, or a Rydberg orbital. In addition, the prime represents a state with a S $1s^{-1}$ core hole, while the states without prime have a S $2p^{-2}$ double core hole. e_{KLL}^- represents the *KLL* Auger electron ejected during the non-radiative relaxation of the *K* hole, and $h\nu$ is the impinging photon. We will report more detail on the resonant-Auger relaxation of the S $1s \rightarrow 6t_{1u}$ excitation in a forthcoming publication. In the present paper, we focus on the dynamics of the relaxation process of the S $1s \rightarrow 6a_{1g}$ forbidden transition.

From Fig. 1, one can see an absorption structure at 2482 eV due to the dipole-forbidden transition of the $1a_{1g}$ electron to the vacant antibonding $6a_{1g}$ state, and the $1s \rightarrow 6t_{1u}$ dipole-allowed resonance at 2486 eV.[17] S 1*s* excitation to Rydberg orbitals are present at higher photon energies.[14] The dipole-forbidden transition has an optical oscillator strength of at least one order of magnitude lower than the dipole-allowed transition.[10] This is in agreement with what is observed in Fig. 1. To rule out significant contributions of quadrupole transitions, we estimated the size of the corresponding matrix elements, which are proportional to $(\vec{k}\cdot\vec{r})^{\ell}$ for the multipole order ℓ. Here, $|\vec{k}| = \frac{2\pi}{\lambda}$, with λ being the wavelength of the x-ray radiation. The integration over $\vec{r}$ makes contributions only in the range of the S 1*s* core hole and we estimated the intensity of the quadrupole transitions to be of the order of 10^{-3} compared to the dipole transitions.

Figure 2 shows the spectrum of the *KLL* resonant Auger transitions in SF_6 measured subsequent to the $1a_{1g} \rightarrow 6a_{1g}$ photoexcitation at 2482 eV. The Auger yield is given in arbitrary units by using a log scale. The resonant *KLL* Auger spectra of SF_6 shown in Figs. 1 and 2 are dominated by $1s^{-1}V' \rightarrow 2p^{-2}(^1S_0, {}^1D_2)V$ transitions.[17] Note that the parent state configuration $2p^{-2}$ can also couple to the final states $^3P_{0,1,2}$; however, transitions to these states are forbidden in LS (i.e., Russell-Saunders) coupling. Because of this only the $1s^{-1}V \rightarrow 2p^{-2}(^3P_2)V$ transitions are barely visible in the spectrum due to intensity borrowing from the $1s^{-1}V \rightarrow 2p^{-2}(^1D_2)V$ transitions by spin–orbit interaction. In addition, strong shake satellites, i.e., transitions from the valence to unoccupied orbitals near the ionization threshold that accompany the $1s^{-1}V \rightarrow 2p^{-2}(^1S_0, {}^1D_2)V$ resonant Auger decays are involved. This observation is similar to the shake transitions during the normal Auger decays of H_2S (see Ref. 24).

Published under an exclusive license by the AVS

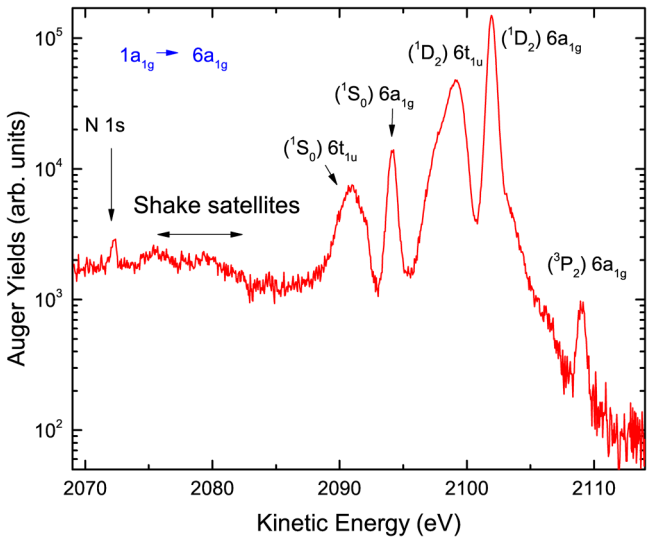

FIG. 2. Overview spectrum of the *KLL* Auger transitions in SF_6 measured subsequent to the $1a_{1g} \rightarrow 6a_{1g}$ photoexcitation at 2482.0 eV. The Auger yield is given in arbitrary units by using a log scale. For more details, see text. The two broad peaks around 2100 and 2092 eV are due to $^1D_2$ and $^1S_0$ Auger lines from the $1a_{1g} \rightarrow 6t_{1u}$ resonance, respectively.

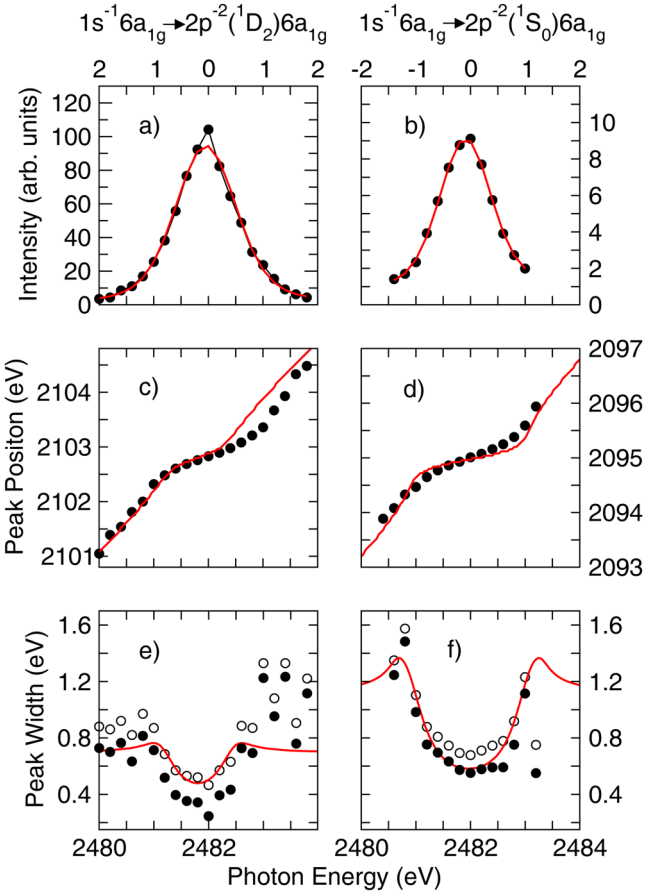

FIG. 3. Results for the resonant Auger decays subsequent to the $1a_{1g} \rightarrow 6a_{1g}$ transition as a function of the incident photon energy detuning from the resonance at 2482 eV. Upper panels: partial electron yield of the (a) $1a_{1g}^{-1}6a_{1g} \rightarrow 2p^{-2}(^1D_2)6a_{1g}$ and (b) $1a_{1g}^{-1}6a_{1g} \rightarrow 2p^{-2}(^1S_0)6a_{1g}$ transition. The red solid lines through the data points represent fit results discussed in Sec. V. Middle panels: peak positions of (c) $1a_{1g}^{-1}6a_{1g} \rightarrow 2p^{-2}(^1D_2)6a_{1g}$ and (d) $1a_{1g}^{-1}6a_{1g} \rightarrow 2p^{-2}(^1S_0)6a_{1g}$ transition. Lower panels: peak widths of (e) $1a_{1g}^{-1}6a_{1g} \rightarrow 2p^{-2}(^1D_2)6a_{1g}$ and (f) $1a_{1g}^{-1}6a_{1g} \rightarrow 2p^{-2}(^1S_0)6a_{1g}$ transition. The hollow data points represent the total widths including experimental resolution while the filled data points show the intrinsic widths. For details, see text. The solid lines in (c)–(f) are the best simulations using Eq. (13).

The $1a_{1g} \rightarrow 6a_{1g}$ transition is dipole-forbidden but yet has appreciable intensity due to vibronic coupling [see Figs. 1 (red box) and 2]. Due to the fact that the vibrational excitation takes place in an asymmetric vibrational picture so that the final vibrational-electronic (vibronic) state belongs to a symmetry consistent with a dipole transition, the excitation can occur, yet with weak intensity. Figure 3 shows the intensities [panels (a) and (b)], the dispersion of the Auger electron kinetic energy [panels (c) and (d)], and the full width at half maximum (FWHM) [panels (e) and (f)] of the $1s^{-1}6a_{1g} \rightarrow 2p^{-2}(^1S_0, ^1D_2)6a_{1g}$ resonant Auger transitions as a function of the excitation energy around the $1s^{-1} \rightarrow 6a_{1g}$ resonance; all data are extracted by fits from the spectra that form the 2D-map shown in Fig. 1. The transition to the $^3P_2$ state has very low statistics and it is not shown. The dispersion curves [panels (c) and (d)] show the energy position of the maximum of the resonant Auger line as a function of photon energy, where a strong divergence from a linear dispersion is evident, with a peculiar "S-shape," rather than a linear dispersion with the photon energy. This is clearly seen as evidence of nuclear dynamics along the potential-energy curve of the $1a_{1g}^{-1}6a_{1g}$ resonance. In this case, the incident photon energy is not liberated by the system exclusively as the kinetic energy of the Auger electron. A share of the available energy is also imparted to the nuclei of the molecule, provoking the stretching and eventually the rupture of the chemical bond,[2,6] which occurs in the present case during the subsequent steps of the Auger decay. The physical explanation for the narrowing [Figs. 3(e) and 3(f)] of Auger lines may be due to the fact that the relaxation processes take place between dissociative potential-energy surfaces for both the intermediate and final states. The asymmetric peak width distributions [panels (e) and (f)] may be associated with the overlap of the $1s^{-1}6a_{1g}$ and $1s^{-1}6t_{1u}$ states in the high photon energy region of Fig. 3, rendering a determination of the $1s^{-1}6a_{1g}$ linewidth difficult. This holds, in particular, for the $1s^{-1}6a_{1g} \rightarrow 2p^{-2}(^1D_2)6a_{1g}$ Auger transition at ≅2102 eV kinetic energy, which has resonances in close vicinity at both sides so that the baseline and, as consequence, the width is difficult to extract; this will become important for the data analysis presented below.

Although the understanding of the S-shape-like dispersion and the behavior of the linewidth as a function of the photon energy (see Fig. 3) is developed for diatomic or quasidiatomic molecules where nuclear dynamics can be understood with an effective dissociative degree of freedom along the S–F axis, the correct

Published under an exclusive license by the AVS

generalization to polyatomic molecules, such as SF_6, with several dissociative degrees of freedom, needs the addition of multidimensional Franck–Condon factors.[25]

Subsequent to the S $1a_{1g}^{-1} \rightarrow 6a_{1g}$ excitation, SF_6 goes through a fast breakup.[10] The excitation of the $1a_{1g}$ electron leads to a state with a repulsive potential (σ^* type) along the S–F bonding. The repulsion gives the fragments a kick such that a substantial change in the geometry of the molecule takes place within a few fs, i.e., during the Auger cascade, while the $6a_{1g}$ orbital is populated.

IV. THEORETICAL PREREQUISITES FOR THE DATA ANALYSIS

S-shape-like features in the 2D maps (see Figs. 1 and 3) are an indication of dissociative intermediate and final states. In the literature, their existence is explained for dipole-allowed intermediate states.[26] We find such features also for the dipole-forbidden S $1s \rightarrow 6a_{1g}$ transition. To explain this finding, we shall first sketch the derivation of the cross section for dipole-allowed excitations and show afterward that for dipole-forbidden resonances cross sections of similar mathematical structure can be derived.

The double differential cross section for the resonant Auger decay is given in its general form by[26]

$$\sigma(\omega, \omega') \propto \sum_f |F_f|^2 \cdot \delta(\omega - \omega' - \omega_{fo}), \tag{1}$$

with

$$F_f = \sum_c \frac{\langle \Psi_f | \mathbf{Q} | \Psi_c \rangle \langle \Psi_c | \mathbf{D} | \Psi_o \rangle}{\omega - \omega_{co} + i\Gamma_c}. \tag{2}$$

Here, ω is the energy of the incoming photon, ω' is the energy of the outgoing photon or electron(s), ω_{co} is the energy difference between the ground state $|o\rangle$ and the core-excited state $|c\rangle$, ω_{fo} is the energy difference between the ground state $|o\rangle$ and the final state $|f\rangle$, $\mathbf{D}$ is the dipole operator for the excitation, $\mathbf{Q}$ is the decay operator, and Γ_c the HWHM of the core-hole lifetime broadening. The δ-function ensures energy conservation for the case of a final state with an infinite lifetime.

In the following, we assume only one electronic final state that allows us to neglect in Eq. (1) the sum over f. Moreover, for dipole-allowed transitions far away from avoided crossings, we can use the Born–Oppenheimer approximation. As a criterion for this approximation, $\hbar\omega_{vib} \ll |E_{el,m} - E_{el_n}|$, with $\hbar\omega_{vib}$ being the vibrational energies and $|E_{el,m} - E_{el,n}|$ being the energetic difference of the electronic states can be used.[27] In the case of SF_6, the vibrational energies are of the order of 100 meV or even less, while the energy splitting between the $1s^{-1}6a_{1g}$ at $h\nu = 2482$ eV and the $1s^{-1}6t_{1u}$ states $h\nu = 2486$ eV amounts approximately to 4 eV (see the 2D-map in Fig. 1) so that the condition can be considered fulfilled. Because of this, we can factorize the electronic and nuclear degrees of freedom such that $|\Psi_i\rangle$ $(i = o, c, f)$ from the Eq. (1) can be rewritten as $|\Psi_i\rangle = |\Phi_i\rangle|\chi_i\rangle$. $|\Phi_i\rangle$ represents the electronic wavefunction as defined previously and $|\chi_i\rangle$ is the nuclear wavefunction. In this approximation, Eq. (1) can be rewritten as

$$\sigma(\omega, \omega') \propto |\mathbf{Q}_{\mathbf{el}}|^2 |\mathbf{D}_{\mathbf{el}}|^2 \left| \sum_c \frac{\langle \chi_f | \chi_c \rangle \langle \chi_c | \chi_o \rangle}{\omega - \omega_{co} + i\Gamma_c} \right|^2 \delta(\omega - \omega' - \omega_{fo}). \tag{3}$$

Here, $\mathbf{D}_{\mathbf{el}} = \langle \Phi_c | D | \Phi_o \rangle$ and $\mathbf{Q}_{\mathbf{el}} = \langle \Phi_f | Q | \Phi_c \rangle$ are the matrix elements for the electronic transitions. In the following, we consider the case of a bound ground state as well as dissociative intermediate and finals states with the approximation of constant slopes F_c and F_f for the potential energy curves, respectively. This allows us to apply for the bound ground state a Gaussian distribution for the vibrational wavefunction χ_o as well as for the wavefunctions χ_i and χ_f of the dissociative intermediate and finals states, respectively, δ-like functions located at the classical turning points of the corresponding potential energy curves. In this way, an analysis of the matrix elements $\langle \chi_f | \chi_c \rangle$ and $\langle \chi_c | \chi_o \rangle$ leads to[28]

$$\sigma(\omega, \omega') \propto |\mathbf{Q}_{\mathbf{el}}|^2 |\mathbf{D}_{\mathbf{el}}|^2 \frac{\exp\left[-\left(\frac{\omega - \omega' - \omega_{fo}(R_0)}{\gamma_f} \right)^2 \right]}{\left(\omega - \omega_{co}(R_0) - \frac{F_c}{F_f}(\omega - \omega' - \omega_{fo}(R_0)) \right)^2 + \Gamma_c^2}. \tag{4}$$

Here, γ_f is the Franck–Condon width of the final state. Moreover, $\omega_{co}(R_0)$ and $\omega_{fo}(R_0)$ represent the energy differences between the corresponding states at the equilibrium distance R_0. The last term of Eq. (4) consists of a product of a Gaussian and a Lorentzian function that, in general, do not have their centroids at the same energy. Because of this, the resulting line shapes are generally asymmetric. For the case that $\gamma_f \gg \Gamma_c$, the S-shapes in 2D-maps can be derived (see, e.g., Ref. 29). In contrast to this, $\gamma_f \ll \Gamma_c$ results in a linear dispersion. Note that similar behavior can be observed for resonant Auger lines of atoms, where the line shapes are also described by a product of a Lorentzian due to the core-hole lifetime and a Gaussian that represents the photon bandwidth.[29,30] In the case of resonant Auger lines of atoms, a transition between the two cases can be obtained by improving the experimental resolution. In contrast to this, in the molecular case of dissociative states, the width of the Gaussian is the product of the spatial spread of the vibrational wavefunction in the ground state and the slope of the potential-energy curve of the dissociative state, i.e., a physical quantity that cannot be changed. Finally, we want to point out that the line shape effect due to the experimental resolution is of minor importance in the present study since the photon bandwidth is smaller than the Lorentzian width caused by the core-hole lifetime.

In the following, we will derive for forbidden transitions an equation, which has a structure similar to Eq. (3), however, with $|\mathbf{D}_{\mathbf{el}}|^2$ replaced by other quantities. This formula is analogous to Eq. (4) and shows that an S-shape-like dispersion can also occur for a dipole-forbidden transition.

In the first step, we will analyze the electronic matrix element $M(Q) = \langle \Phi_c(Q) | \mathbf{D} | \Phi_o(Q) \rangle$ in more detail. For this purpose, we have to consider that the molecular wavefunctions Ψ depend on i normal modes Q_i and j electronic coordinates q_j. Moreover, Q is the vector formed by the normal modes Q_i. In this way, we obtain

Published under an exclusive license by the AVS

for the electronic matrix element,[31]

$$M(Q) = \langle \Phi_c(q, Q)|\mathbf{D}|\Phi_o(q, Q)\rangle = M(Q_0) + \sum_i \left(\frac{\partial M(Q)}{\partial Q_i}\right)_{Q_0} Q_i + \frac{1}{2}\sum_{i,i'}\left(\frac{\partial^2 M(Q)}{\partial Q_i \partial Q_{i'}}\right)_{Q_0} Q_i Q_{i'} + \cdots. \quad (5)$$

Here, Q_0 describes the equilibrium geometry in the initial state of the transition. With this formula, we obtain for the vibronic transitions,[31]

$$M_{\chi_c\chi_o}(Q) = \langle \chi_c(Q)|M(Q)|\chi_o(Q)\rangle = M(Q_0)\langle \chi_c(Q)|\chi_o(Q)\rangle + \sum_i \left(\frac{\partial M(Q)}{\partial Q_i}\right)_{Q_0} \langle \chi_c(Q)|Q_i|\chi_o(Q)\rangle + \frac{1}{2}\sum_{i,i'}\left(\frac{\partial^2 M(Q)}{\partial Q_i \partial Q_{i'}}\right)_{Q_0} \langle \chi_c(Q)|Q_i Q_{i'}|\chi_o(Q)\rangle + \cdots, \quad (6)$$

with $|\chi(Q)\rangle$ being the product of the vibrational wavefunctions of all normal modes Q_i. Note that $M(Q_0)$ is identical to $\mathbf{D}_{el}$ in Eq. (3), where the higher-order corrections of Eq. (6) are neglected.

In the next step, we specify Eq. (6) for a dipole-forbidden transition, i.e., we assume $M(Q_0) = 0$, and we take only first-order corrections into account. Moreover, we take into account two vibrational modes, namely, one symmetry-conserving mode Q_1 (which is in the case of SF_6 the symmetric stretching mode a_{1g}) and one symmetry-lowering mode Q_2, the so-called promoting mode. Actually, according to Ref. 10 in the case of SF_6 mainly the asymmetric stretching and to a lower extent the bending mode, both with symmetry t_{1u}, are responsible for the excitation of the $1s^{-1}6a_{1g}$ state, i.e., we simplify the problem compared to reality, however, without loss of information. In this way, we obtain with $|\chi(Q)\rangle = |\chi(Q_1)\rangle|\chi(Q_2)\rangle$,

$$M_{\chi_c\chi_o}(Q) = \left(\frac{\partial M(Q)}{\partial Q_1}\right)_{Q_0} \langle \chi_c(Q_1)|Q_1|\chi_o(Q_1)\rangle\langle \chi_c(Q_2)|\chi_o(Q_2)\rangle + \left(\frac{\partial M(Q)}{\partial Q_2}\right)_{Q_0} \langle \chi_c(Q_2)|Q_2|\chi_o(Q_2)\rangle\langle \chi_c(Q_1)|\chi_o(Q_1)\rangle. \quad (7)$$

In the following, we argue that $\left(\frac{\partial M(Q)}{\partial Q_1}\right)_{Q_0} = 0$ since the considered electronic transition is dipole-forbidden in the given symmetry, i.e., a change along the symmetry-conserving mode will not result in an allowed transition. In this way, we can simplify the equation to

$$M_{\chi_c\chi_o}(Q) = \left(\frac{\partial M(Q)}{\partial Q_2}\right)_{Q_0} \langle \chi_c(Q_2)|Q_2|\chi_o(Q_2)\rangle\langle \chi_c(Q_1)|\chi_o(Q_1)\rangle. \quad (8)$$

Here, $\langle \chi_c(Q_2)|Q_2|\chi_o(Q_2)\rangle$ describes excitations of the nontotally symmetric mode.

In the following, we discuss the matrix elements $\langle \chi_c(Q_2)|Q_2|\chi_o(Q_2)\rangle$ in more detail. Both the ground state and the excited state $1s^{-1}6a_{1g}$ have A_{1g} symmetry so that it cannot undergo any symmetry lowering due to a Jahn–Teller effect. Because of this, we assume that its geometry is at least close to octahedral, i.e., there are no major changes in the equilibrium values for the nontotally symmetric modes upon the Auger transition. Because of this, we can assume that for both states the potential-energy curves along this normal mode are parallel, i.e., $\langle \chi_c(Q_2)|\chi_o(Q_2)\rangle = \delta_{\nu_o(Q_2),\nu_c(Q_2)}$ with $\nu_o(Q_2)$ and $\nu_c(Q_2)$ being the vibrational quantum numbers for the asymmetric mode in the ground and in the core-excited state. As a result, the matrix element $\langle \chi_c(Q_2)|Q_2|\chi_o(Q_2)\rangle$ matches in its structure those of molecular vibrational transitions induced by infrared radiation, with the selection rule $\Delta\nu = \pm 1$ for harmonic oscillator potentials.[32]

Due to the vibrational energies of the relevant asymmetric modes, which are larger than k_bT with k_b being the Boltzmann constant and T the temperature, we can assume that in the electronic ground state, the vibrational ground states of these modes, $\chi_{\nu_o=0}$, are populated. Because of this only the matrix element,

$$\langle \chi_{\nu_c=1}(Q_2)|Q_2|\chi_{\nu_o=0}(Q_2)\rangle = \frac{a}{\sqrt{2}}, \quad (9)$$

with $a = \frac{1}{\sqrt{\mu_2\omega_{vib,2}}}$ has to be taken into account. Here, $\omega_{vib,2}$ is the vibrational energy and μ_2 is the respective reduced mass of the asymmetric mode; the latter quantity can be calculated according to an algorithm given by Wilson *et al.*[33] In this way, we obtain for the excitation matrix element,

$$M_{\chi_c=1,\chi_o=0}(Q) = \left(\frac{\partial M(Q)}{\partial Q_2}\right)_{Q_0} \cdot \frac{a}{\sqrt{2}} \cdot \langle \chi_c(Q_1)|\chi_o(Q_1)\rangle, \quad (10)$$

i.e., it is proportional to the derivative of the transition dipole moment and the spatial extension of the vibrational wavefunction of the lowest vibrational state of the symmetry breaking of the nontotally symmetric mode.

With Eq. (10), we obtained the first important result for the present study, namely, that the matrix element for the excitation consists of the Franck–Condon factors for the symmetric stretching mode, which are multiplied by a constant value. This allows us to derive from the intensities shown in Figs. 3(a) and 3(b) the slope of the core-excited state (see below).

In the following part, we will consider the Auger decay, which is allowed according to the corresponding selection rules, so that the leading term of the matrix element is given by

$$M^{decay} = \mathbf{Q}_{el}\langle \chi_f(Q_2)|\chi_c(Q_2)\rangle\langle \chi_f(Q_1)|\chi_c(Q_1)\rangle. \quad (11)$$

The final state of the $1s^{-1}6a_{1g} \rightarrow 2p^{-2}(^1S_0)6a_{1g}$ Auger decay has also A_{1g} symmetry so that we can use with the above-given arguments $\langle \chi_f(Q_2)|\chi_c(Q_2)\rangle = \delta_{\nu_c(Q_2),\nu_f(Q_2)}$, with $\nu_f(Q_2)$ being the vibrational quantum of the nontotally symmetric mode in the final state. The Auger final states $2p^{-2}(^1D_2)6a_{1g}$ possess either E_g or T_{2g} symmetry so that we cannot make the same conclusion in a straight-forward way. However, the results in Figs. 3(c) and 3(d) are similar to those for the transitions to the $1s^{-1}6a_{1g} \rightarrow 2p^{-2}(^1S_0)6a_{1g}$ state so that we also conclude that no significant distortion exists for the final states with E_g and T_{2g} symmetry. With the above mentioned selection rule $\Delta\nu = \pm 1$ for the promoting mode Q_2 in the course of the excitation process and the just mentioned δ-function, we obtain

Published under an exclusive license by the AVS

that only the vibrational level $v_f(Q_2) = 1$ can be populated in the electronic final state.

In this way, we obtain in the lowest nonvanishing order for the excitation and decay process,

$$\begin{aligned}
\sigma(\omega,\omega') \propto |M_{\chi_c=1\chi_o=0}(Q)\cdot M^{decay}|^2 &= \left|\left(\frac{\partial M(Q)}{\partial Q_2}\right)_{Q_0}\right|^2 |\mathbf{Q}_{\mathrm{el}}|^2 \\
&\times \left|\sum_c \frac{\langle\chi_f(Q_2)|\chi_c(Q_2)\rangle\langle\chi_c(Q_2)|Q_2|\chi_o(Q_2)\rangle\langle\chi_f(Q_1)|\chi_c(Q_1)\rangle\langle\chi_c(Q_1)|\chi_o(Q_1)\rangle}{\omega-\omega_{co}+i\Gamma_c}\right|^2 \times \delta(\omega-\omega'-\omega_{fo}) \\
&= \left|\left(\frac{\partial M(Q)}{\partial Q_2}\right)_{Q_0}\right|^2 \frac{a^2}{2}|\mathbf{Q}_{\mathrm{el}}|^2 \times \left|\sum_c \frac{\langle\chi_f(Q_1)|\chi_c(Q_1)\rangle\langle\chi_c(Q_1)|\chi_o(Q_1)\rangle}{\omega-\omega_{co}+i\Gamma_c}\right|^2 \delta(\omega-\omega'-\omega_{fo}) \\
&= \left|\left(\frac{\partial M(Q)}{\partial Q_2}\right)_{Q_0}\right|^2 \frac{a^2}{2}|\mathbf{Q}_{\mathrm{el}}|^2 \times \frac{\exp\left[-\left(\frac{\omega-\omega'-\omega_{fo}(R_0)}{\gamma_f}\right)^2\right]}{\left(\omega-\omega_{co}(R_0)-\frac{F_c}{F_f}(\omega-\omega'-\omega_{fo}(R_0))\right)^2+\Gamma_c^2} \\
&\cong \left|\left(\frac{\partial M(Q)}{\partial Q_2}\right)_{Q_0}\right|^2 \frac{a^2}{2}|\mathbf{Q}_{\mathrm{el}}|^2 \times \frac{\exp\left[-\left(\frac{\omega-\omega'-\omega_{fo}(R_0)}{\gamma_f}\right)^2\right]}{(\omega'-\omega_{cf}(R_0))^2+\Gamma_c^2}. \qquad (12)
\end{aligned}$$

The last transformation is obtained by performing the same rearrangements as from Eq. (3) to Eq. (4). The approximation in the last line is based on the simplification that the slopes of the potential-energy curves of the intermediate and the final state are identical, i.e., $F_c = F_f$; this is fulfilled for RIXS, while for resonant Auger the second from last line has to be used. Note that the cross section in the last two lines has the same mathematical structure as that in Eq. (4), which allows us to obtain S-shape-like dispersion relations.

In the data analysis, we used the fourth line of Eq. (12) with different slopes of the intermediate and the final state as realized in resonant Auger spectroscopy. Nevertheless, we use in the following discussion the last line of Eq. (12) since the simplified denominator $(\omega'-\omega_{cf}(R_0))^2+\Gamma_c^2$ makes the arguments clearer. Note that the ratio $F_c/F_f \cong 0.8$, see below, is sufficiently close to 1 so that it does not have an influence on the following argumentation. The two main differences between Eq. (4) and the last line of Eq. (12) are given by the meaning of $\omega_{fo}(R_0)$. For Eq. (4), it is given by $\omega_{fo}(R_0) = E_f(R_0) - E_0(R_0)$, i.e., the energy difference between the potential-energy curves at the equilibrium geometry of the ground state. In the case of the last line, Eq. (12) holds $\omega_{fo}(R_0) = E_f(R_0) - E_0(R_0) + \hbar\omega_{vib,2}$, i.e., one additional energy quantum of the asymmetric mode has to be added.

Up to now, we considered one promoting asymmetric mode. However, for SF_6, two such modes exist with t_{1u} symmetry, namely, the more important asymmetric stretching mode with a vibrational energy of ≅120 meV and the less important bending mode with a vibrational energy of ≅75 meV with an intensity ratio of the contributions of ≅3 : 1 (see Ref. 10). These two promoting modes lead to the excitation of different vibrational levels in the core-excited and the final state so that lifetime interference contributions can be neglected. As a result, the cross section can be written as

$$\sigma(\omega,\omega') = \sum_{i=1}^{2}\left|\left(\frac{\partial M(Q)}{\partial Q_{2,i}}\right)_{Q_0}\right|^2 \frac{a_i^2}{2}|\mathbf{Q}_{\mathrm{el}}|^2 \times \frac{\exp\left[-\left(\frac{\omega-\omega'-\omega_{fo,i}(R_0)}{\gamma_f}\right)^2\right]}{(\omega'-\omega_{cf}(R_0))^2+\Gamma_c^2}. \qquad (13)$$

Here, i are the two different active asymmetric modes. The different values for a_i and $\left(\frac{\partial M(Q)}{\partial Q_{2,i}}\right)_{Q_0}$ lead just to different strong contributions caused by the different active modes. Finally, the cross section in Eq. (13) was convoluted with a Lorentzian to account for the finite lifetime Γ_f of the $2p^{-2}6a_{1g}$ final states (see Refs. 2 and 28).

In the following, we consider the numerator and denominator of the last term. In the numerator, the excitation of vibrational levels of the asymmetric vibrational mode leads to a shift of $\omega_{fo}(R_0)$ by the corresponding vibrational energy. This amounts in the case of SF_6 ≅ 120 meV for one quantum of the most important mode (asymmetric stretching mode) and ≅75 meV for the second relevant mode (bending mode)[10] and leads to a corresponding shift of the Gaussian in the numerator, see above. In contrast to this, for the Auger transition, we assume that $\langle\chi_f(Q_2)|\chi_c(Q_2)\rangle = \delta_{v_c(Q_2),v_f(Q_2)}$ (see also above). Because of this, $\omega_{cf}(R_0)$ changes only by the difference of the vibrational energy of the asymmetric mode in the core-excited and the final state, i.e., the denominator remains almost unchanged. From this, we conclude that in the case of a dipole-forbidden transition with two active nonsymmetric modes, we observe two dispersion relations, which exhibit the same shape, but are shifted relative to each other by some meV in terms of the Auger energy and some 10 meV, namely, the difference of the vibrational energies of the two active modes, in terms of the

Published under an exclusive license by the AVS

photon energy. These values for the shifts are small compared to other quantities like lifetime broadening or experimental resolution and, as a consequence, the differences between the two dispersion relations can safely be neglected. Because of this, an S-shape-like spectral feature in a 2D-map can be described with the last line of Eq. (12). Because of this, from the S-shape-like dispersion curves displayed in Figs. 3(c) and 3(d) and linewidths behavior of the resonant Auger peaks shown in Figs. 3(e) and 3(f), the quantities γ_f and Γ_c can be extracted in both cases, i.e., the dipole-allowed and the dipole-forbidden transition. In Sec. V, the data analysis for the $1a_{1g}^{-1}6a_{1g} \rightarrow 2p^{-2}6a_{1g}$ decay will be reported.

V. DATA ANALYSIS AND DISCUSSION

In the following, we shall analyze in more detail the results presented graphically in Fig. 3 in order to obtain slopes of the potential-energy curves. Figures 3(a) and 3(b) show the intensities of the S $1s^{-1}6a_{1g} \rightarrow 2p^{-2}6a_{1g}$ resonant Auger decays as a function of the photon energy as obtained from the 2D-map presented in Fig. 1 and represent the relative absorption cross section of the $1s^{-1}6a_{1g}$ core-excited states. In contrast to conventional photoabsorption spectra, the 2D-map allows separating this weak excitation from the background formed by the tails of the $1s^{-1}6t_{1u}$ core excitation. This provides the opportunity to derive the slope of the corresponding potential-energy curves.

For this purpose, the PEYs shown in Figs. 3(a) and 3(b) are fitted with a Lorentzian line shape convoluted by a Gaussian shape that describes the Franck–Condon width and the experimental resolution. As Lorentzian width, a value of $2\Gamma_c = 0.55$ eV was used to account for the S $1s^{-1}$ core-hole lifetime.[21] The Gaussian width was a free parameter, which resulted in a value of 875(50) meV FWHM. By assuming a photon bandwidth of 375 meV, the Franck–Condon width γ_c of the core-excited state resulted in 822(55) meV FWHM.

Using the *Condon-Reflexion principle*,[34] one can relate the Franck–Condon width to the spatial width of the respective vibrational wave function in the electronic ground state of the molecule, which is in the given case the symmetric stretching vibration. In this case, the slope of the potential of the core-excited state $1s^{-1}6a_{1g}$ is given by $F_c = -b\gamma_c$ (see Ref. 35). Here, F_c is the slope along the internuclear distance r between the S and the F atoms. Moreover, $b^2 = \frac{6\mu\omega_{vib,1}}{\hbar}$, with μ being the mass of a F atom and $\omega_{vib,1}$ the frequency of the symmetric stretching mode. The factor 6, which is absent in the case of a diatomic molecule, is due to the six equivalent S–F bond distances in the symmetric stretching mode. Finally, γ_c is defined by the Gaussian function,

$$I(E) \propto \frac{1}{\sqrt{\pi}\gamma_c} e^{-\left(\frac{E-E_0}{\gamma_c}\right)^2}, \tag{14}$$

with E_0 being the resonance energy. The Franck–Condon width (FWHM) of the Gaussian is given by $\sqrt{4\ln 2}\,\gamma_c \cong 1.67\,\gamma_c$ so that the slope of the core-excited state $1s^{-1}6a_{1g}$ is given by $F_c = -b\gamma_c = -25.3(1.8)$ eV/Å. For more details on calculating slopes in polyatomic molecules as well as when higher vibrational levels (e.g., hot bands) have to be taken into account, see Ref. 35.

From the derived slope and the fact that six F atoms are accelerated, we derived in a classical picture within the core-hole lifetime of $\cong 1.1$ fs a bond elongation of $\cong 0.007$ Å, i.e., a change which is small compared to the equilibrium bond distance of 1.564 Å.

In the next step, we derive from the energy positions and widths shown in Figs. 3(c)–3(f) the slopes of the S $2p^{-2}6a_{1g}$ states at the equilibrium distance of the ground state. For this purpose, the experimental curves shown in these panels are fitted using the fourth line of Eq. (12) convoluted with a Lorentzian to account for the finite lifetime Γ_f of the final state. Since Eq. (13) does not take into account the experimental resolution, prior to the fit the intrinsic widths of the peaks (full data points) are estimated based on the experimentally observed widths (hollow data points). In detail, the experimental peak width ΔE_{exp} consists of three contributions, namely, the intrinsic width ΔE_{in}, the analyser resolution ΔE_{ana}, and the contribution of the photon bandwidth ΔE_{photon}. The analyser resolution can be approximated with a Gaussian function with a width of $\Delta E_{ana} = 375$ meV. The contributions of the photon bandwidth ΔE_{photon} can also be approximated with a Gaussian. It is given by the product of the photon bandwidth of 300 meV multiplied by the slope of the energy dispersion of the respective spectral feature.[28,36] The slope can be derived from Figs. 3(c) and 3(d) and assumes the different photon energies values between 0.37 and 1.23 resulting in $\Delta E_{photon} = 110$–370 meV. As can be seen from Eq. (13), the intrinsic line shape is given by a product of a Lorentzian and a Gaussian, however, in general with different centroids for the two contributions. To obtain the intrinsic width, the relation $\Delta E_{\text{exp}}^2 = \Delta E_{in}^2 + \Delta E_{ana}^2 + \Delta E_{photon}^2$ is applied, although it is strictly valid only for pure Gaussian line shapes.

For the fits of the energy dispersions and intrinsic widths (filled data points) shown in Figs. 3(c)–3(f) a core-hole lifetime of $2\Gamma_c = 550$ meV[21] and $2\Gamma_f = 140$ meV was used. The latter value is based on the relation that for shallow core levels the double-core-hole lifetime broadening is about 2.8 times the lifetime broadening of single core holes[37,38] and a lifetime width of $2\Gamma \cong 50$ meV for the S 2p core hole.[7]

From the fits, we obtained slopes of $F_f = -18.9(1.0)$ eV/Å and $-31.7(1.1)$ eV/Å for the $2p^{-2}(^1D_2)6a_{1g}$ and $2p^{-2}(^1S_0)6a_{1g}$ final states, respectively. Obviously, both values are in a reasonable range for slopes of dissociative potential energy curves. However, we expect similar slopes for these two states since the molecular bond character and the potential-energy curves are formed by the valence orbital occupation, which is identical for these two states. With this assumption, the two obtained slopes disagree significantly within the error bars so that we shall discuss the results in the following.

As already discussed above and visible in Figs. 1 and 2, the $1s^{-1}6a_{1g} \rightarrow 2p^{-2}(^1S_0)6a_{1g}$ resonant Auger transition is rather well isolated while the $1s^{-1}6a_{1g} \rightarrow 2p^{-2}(^1D_2)6a_{1g}$ transition is encircled by a number of rather intense resonant Auger transitions. Because of this, for the latter transitions, the peak parameters, and, in particular, the widths are more difficult to extract with high accuracy. This is probably the reason why the fits describe the widths of the $1s^{-1}6a_{1g} \rightarrow 2p^{-2}(^1S_0)6a_{1g}$ transitions [Fig. 3(f)] much better than for the $1s^{-1}6a_{1g} \rightarrow 2p^{-2}(^1D_2)6a_{1g}$ transitions [Fig. 3(e)]. Finally, we expect a larger slope for a double-core-hole state than for a single-core-hole state, which is only given for the result of the

Published under an exclusive license by the AVS

$2p^{-2}(^1S_0)6a_{1g}$ final state. From these results, we conclude that the slope of −31.7(1.1) eV/Å for the $2p^{-2}(^1S_0)6a_{1g}$ final state is reliable, while the slope of −18.9(1.0) eV/Å for the $2p^{-2}(^1D_2)6a_{1g}$ final state is due to a poor extraction of the peak widths due to overlapping transitions. As already proposed in a recent publication,[28] this suggests developing codes that allow fitting entire 2D-maps as shown in Fig. 1. Such approaches will allow extracting parameters of strongly overlapping peaks with high accuracy; they are, however, beyond the scope of the present work.

VI. CONCLUSIONS

In this paper, we have used a core-hole-clock method, namely, resonant Auger emission, to observe dynamical phenomena in the analysis of the S $1s^{-1}(1a_{1g}^{-1}) \rightarrow 6a_{1g}$ symmetry-forbidden resonant excitation of SF_6 and subsequent *KLL* Auger relaxation using state-of-the-art experimental resolution. The dynamic symmetry breaking is validated through the investigation of electronically dipole-forbidden transitions. An S-shape for the kinetic energy dispersion of the Auger electrons is observed. For dipole-allowed transitions, such S-shapes originate from dissociative core-hole and final states; they allow us to derive the potential slopes of the states involved. We show that this is also valid for the present case of the dipole-forbidden S $1s^{-1}(1a_{1g}^{-1}) \rightarrow 6a_{1g}$ resonance. Based on this result, we derived the slope of the S $1s^{-1}6a_{1g}$ state to be −25.3(1.8) eV/Å and for the S $2p^{-2}6a_{1g}$ state to be −31.7(1.1) eV/Å.

Finally, we want to emphasize that the present validation for using the properties of S-shapes dispersion for dipole-forbidden transitions is based on the Born–Oppenheimer approximation, i.e., it is only valid when the energy splitting between electronic states is much larger than the vibrational energies. From this directly follows that the present arguments are generally not valid for dipole-forbidden transitions, which may undergo a strong Jahn–Teller distortion. Nevertheless, the present case of the forbidden S $1s^{-1}(1a_{1g}^{-1}) \rightarrow 6a_{1g}$ excitation in SF_6 is not an isolated finding. Similar excitations are, e.g., Si $1s^{-1} \rightarrow 6a_1$ in SiF_4[39,40] and Si $1s^{-1} \rightarrow 8a_1$ in $SiCl_4$.[41] From this, we expect that the present situation is quite common in highly symmetric molecules, where dipole-forbidden transitions are common due to the corresponding strict selection rules.

ACKNOWLEDGMENTS

A.C.F.S. acknowledges support from CNPq and CAPES. Experiments were performed on the GALAXIES beamline at SOLEIL Synchrotron, France (Proposal No. 20170368). The authors are grateful to D. Prieur for technical assistance and to SOLEIL staff for smoothly running the facility. D.K. wishes to acknowledge financial support from LabEx MiChem, France as well as the Swedish Research Council (VR) and the Knut and Alice Wallenberg Foundation, Sweden.

AUTHOR DECLARATIONS

Conflict of Interest

The authors have no conflicts to disclose.

DATA AVAILABILITY

The data that support the findings of this study are available from the corresponding author upon reasonable request.

REFERENCES

[1]M. Simon *et al.*, Phys. Rev. A **73**, 1781 (2006).
[2]T. Marchenko *et al.*, Phys. Rev. Lett. **119**, 133001 (2017).
[3]N. Boudjemia *et al.*, Phys. Chem. Chem. Phys **22**, 26806 (2020).
[4]M. N. Piancastelli, T. Marchenko, R. Guillemin, L. Journel, O. Travnikova, I. Ismail, and M. Simon, Rep. Prog. Phys. **83**, 016401 (2020).
[5]L. Young *et al.*, J. Phys. B **51**, 032003 (2018).
[6]M. N. Piancastelli *et al.*, J. Phys. B **50**, 042001 (2017).
[7]M. O. Krause and J. H. Oliver, J. Phys. Chem. Ref. Data **8**, 329 (1979).
[8]O. Travnikova *et al.*, Phys. Rev. Lett. **116**, 213001 (2016).
[9]V. Ekholm *et al.*, J. Phys. B **53**, 185101 (2020).
[10]A. Gomes, R. Oliveir, A. Rocha, W. Wolff, K. Alcantara, G. Sigaud, and A. Santos, Int. J. Mass Spectrom. **388**, 9 (2015).
[11]E. Hudson, D. A. Shirley, M. Domke, G. Remmers, A. Puschmann, T. Mandel, C. Xue, and G. Kaindl, Phys. Rev. A **47**, 361 (1993).
[12]T. A. Ferrett, M. N. Piancastelli, D. W. Lindle, P. H. Heimann, L. H. Medhurst, S. H. Liu, and D. A. Shirley, Chem. Phys. Lett. **134**, 146 (1987).
[13]T. A. Ferrett, D. W. Lindle, P. A. Heimann, M. N. Piancastelli, P. H. Kobrin, H. G. Kerkhoff, U. Becker, W. D. Brewer, and D. A. Shirley, J. Chem. Phys. **89**, 4726 (1988).
[14]C. Reynaud, M.-A. Marc-André Gaveau, K. Bisson, I. Millié, P. Nenner, S. Bodeur, P. Archirel, and B. Lévy, J. Phys. B **29**, 5403 (1996).
[15]R. Feifel *et al.*, Sci. Rep. **7**, 6513 (2017).
[16]H. Nakamatsu and T. Mukoyama, J. Chem. Phys. **95**, 3167 (1991).
[17]T. A. Ferrett, D. W. Lindle, P. A. Heimann, H. G. Kerkhoff, U. E. Becker, and D. A. Shirley, Phys. Rev. A **34**, 1916 (1986).
[18]J.-P. Rueff *et al.*, J. Synchrotron Rad. **22**, 175 (2015).
[19]J. Tulkki, N. M. Kabachnik, and H. Aksela, Phys. Rev. A **48**, 1277 (1993).
[20]A. Knie, M. Patanen, A. Hans, I. D. Petrov, J. D. Bozek, A. Ehresmann, and P. V. Demekhin, Phys. Rev. Lett. **116**, 193002 (2016).
[21]R. Püttner *et al.* (unpublished).
[22]R. E. LaVilla, J. Chem. Phys. **57**, 899 (1972).
[23]M. Alagia *et al.*, Phys. Rev. A **71**, 63 (2005).
[24]R. Püttner, D. Céolin, R. Guillemin, R. K. Kushawaha, T. Marchenko, L. Journel, M. N. Piancastelli, and M. Simon, Phys. Rev. A **93**, 042501 (2016).
[25]T. Åberg and B. Crasemann, *Resonant Anomalous X-Ray Scattering* (North-Holland, Amsterdam, 1994).
[26]F. Gel'mukhanov and H. Ågren, Phys. Rev. A **54**, 379 (1996).
[27]F. Hagelberg, *Electron Dynamics in Molecular Interactions Principles and Applications* (Imperial College, London, 2014), p. 54.
[28]G. Goldsztejn, R. Guillemin, T. Marchenko, O. Travnikova, D. Céolin, L. Journel, M. Simon, M. N. Piancastelli, and R. Püttner, Phys. Chem. Chem. Phys. **24**, 6590 (2022).
[29]F. Gel'mukhanov and H. Ågren, Phys. Rev. A **54**, 3960 (1996).
[30]E. Kukk, S. Aksela, and H. Aksela, Phys. Rev. A **53**, 3271 (1996).
[31]G. Fischer, *Vibronic Coupling the Interaction between the Electronic and the Nuclear Motion* (Academic Press, London, Orlando, 1984), p. 44.
[32]P. W. Atkins and R. S. Friedman, *Molecular Quantum Mechanics*, 3rd ed. (Oxford University, Oxford, 1997).
[33]E. B. Wilson, J. C. Decius, and P. C. Cross, *Molecular Vibrations, The Theory of Infrared and Raman Vibrational Spectra* (Dover, New York, 1980).
[34]G. Herzberg, *Molecular Spectra and Molecular Structure. I. Spectra of Diatomic Molecules* (Van Nostrand, Princeton, 1950), pp. 392–393.

Published under an exclusive license by the AVS

[35]R. Püttner, T. Arion, M. Förstel, T. Lischke, M. Mucke, V. Sekushin, G. Kaindl, A. M. Bradshaw, and U. Hergenhahn, Phys. Rev. A **83**, 043404 (2011).
[36]R. Guillemin *et al.*, Phys. Rev. A **92**, 238 (2015).
[37]M. Žitnik *et al.*, Phys. Rev. A **93**, 021401(R) (2016).
[38]G. Goldsztejn *et al.*, Phys. Rev. Lett. **117**, 133001 (2016).
[39]O. Takahashi *et al.*, J. Phys. Conf. Ser. **235**, 012018 (2010).
[40]I. H. Suzuki, Y. Kono, A. Ikeda, T. Ouchi, K. Ueda, O. Takahashi, I. Higuchi, Y. Tamenori, and S. Nagaoka, J. Chem. Phys. **134**, 084312 (2011).
[41]I. H. Suzuki, Y. Kono, K. Sakai, M. Kimura, K. Ueda, Y. Tamenori, O. Takahashi, and S. Nagaoka, J. Phys. B **46**, 075101 (2013).

Published under an exclusive license by the AVS